The 19th Conference of Mechanical Engineering Network of Thailand
19-21 October 2005, Phuket, Thailand

Simulations of Stress Wave Propagation from Dynamic Loads

Tarin Vanichayangkuranont[1], Kuntinee Maneeratana[1] and Nuwong Chollacoop[2]
[1] Department of Mechanical Engineering, Chulalongkorn University, Bangkok 10330
[2] National Metal and Materials Technology Center (MTEC), Pathumthani 12120
Email tarinv@yahoo.com, kuntinee.m@chula.ac.th and nuwongc@mtec.or.th

Abstract

Stress waves in solid bodies from dynamic loads are simulated by the ABAQUS finite element package. The considered body geometries are 1D & 2D bars and thick & thin walls. The 2D plane strain condition is assumed. Material properties are elastic and bi-linear elastic plastic with non-linear geometry stipulation. The 1D elastic results are compared with available analytical solutions while the additional effects of geometries and materials are monitored, described and clarified. It is shown that the wave propagations should not be neglected, particularly under very high dynamic loadings. The simulations show that a reasonably fine mesh is required in conjunction with the time increment of an appropriate Courant number Co – fraction of the smallest element that the stress wave travels in one time step. The Co values of up to 0.5 are acceptable but 0.1 is recommended to ensure the grid and time independency solutions.

Keywords: stress wave propagation, Courant number, dynamic loadings, ABAQUS, finite element method

1. Introduction

The National Metal and Materials Technology Center (MTEC) has initiated a project to develop the light weight hard armour for the Royal Thai Military Armoury [1], aiming to improve materials and design, produce and test hard armour prototypes. In the process, materials and design prototypes must be assessed by standard firing tests (Figure 1) which are time consuming and expensive.

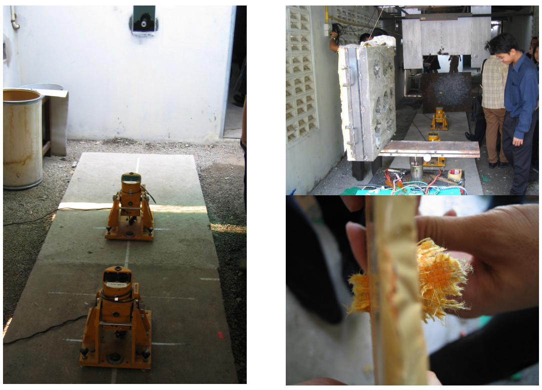

Figure 1 Standard firing tests.

As hard armours comprise of layers of ceramic, steel and polymer plates, the design involves the parameter specification on ceramic tile shape/sizes, thicknesses and arrangements of material layers. The design by trials and errors would require a lot of firing tests on prototypes. Thus, the numerical simulation is proposed as the alternative method of analysing ballistic loads on the armours, obtaining design specifications as well as reducing the number of firing tests. The advantages of the method include the cost and time reduction in the design process with the suggested guidelines, particularly parameter adjustments for the optimised configuration.

These simulations must contain many complex models, including the impact of deformable bullets on the armour, large deformation of materials with various degrees of strain-rate sensitivities, stress waves and material failure modes from bullet penetration. It is the modelling of stress wave that is the focus of this paper.

In dynamic impact problems, there are shock waves travelling through the solid medium in very much the same way as in fluids, but at a much higher velocity. For instance, when a ship is subjected to a underwater explosion, the detonation produces a shock wave moving from the source at the speed of around 1500 m/s [2]. However, when the shock reaches the ship and the energy is transferred to the hull, the elastic wave speed in the steel approaches 5000 m/s, resulting in a much faster shock front and more complicate wave reflection and superposition. This discrepancy of wave speeds may be the reason that the solid waves are often ignored [2] as the stress in the solid reaches quasi-static conditions due to wave interference with respect to the time increments of fluid shocks.

Nonetheless, the shock wave propagation and superposition in solids may be neglected at one's own perils. The high explosive squash head (HESH) effect or the high explosive plastic (HEP) method of attacking armour [3] is a prime example of stress wave utilisation in military applications. The detonation of high explosive in contact with the armour plate produces the shock wave travelling through the armour. The superposition of the stress wave at the rear surface of the plate can detach a large scrab at a high velocity of up to 130 m/s. That is, the complete penetration or perforation is not necessary to cause damage as the scrab acts as a projectile on the other side of the plate.

Another example is the use of high performance polymeric fibres – characterised by low density and high strength which help increasing the wave speed – in lightweight armours. High wave speeds in the fibres are greatly desirable as they facilitate a fast and efficient absorption of the impact energy through the enlarged deformed regions [4], [5].

In this study, the conditions for numerical modelling of wave propagations in solids are studied in details, particularly the time increment and grid independency requirements. The ABAQUS finite element package is used to model elastic and bi-linear elastic plastic stress waves in simple geometries – 1D & 2D bars and thick & thin walls. Numerical predictions are then compared with available analytical solutions.

2. ABAQUS Finite Element Package

Relevant parts of the package are mentioned [6].

2.1 ABAQUS/Explicit Package

The ABAQUS/Explicit is used instead of the normal ABAQUS/Standard as the Explicit package is more suitable for the analyses in which high speed, non-linear, transient response dominates the solutions.

2.2 Material Constitutive Models

The elastic and bi-linear elastic plastic isotropic material models are used. In the elastic region, the stress σ_{ij} and strain ε_{ij} relationship are related by 2 material properties: Young's modulus E and the Poisson's ratio ν,

$$\sigma_{ij} = \frac{E}{(1+\nu)}\varepsilon_{ij} + \frac{\nu E}{(1+\nu)(1-2\nu)}\varepsilon_{kk}\delta_{ij}\ , \qquad (1)$$

where δ_{ij} is the Kronecker's delta.

In the plastic region, the simple metal plasticity model with isotropic hardening is employed. The strain rate is decomposed into the elastic *el* and plastic *pl* components. For the yield surface, the von Mises equivalent stress with the associated flow rule are used with the deviatoric stress S_{ij} and strain e_{ij} such that,

$$S_{ij} = \frac{E}{1+\nu}e^{el}_{ij}\ ,\ de^{el}_{ij} = d\overline{e}^{\,pl}\frac{\sqrt{3}S_{ij}}{\sqrt{2S_{kl}S_{kl}}}\ , \qquad (2)$$

where $d\overline{e}^{\,pl}$ is the equivalent plastic strain rate.

In addition, the geometrically non-linear analysis with large displacements, the NLGEOM option, is used. Elements are formulated in the current configuration using current nodal positions. Strains are calculated as the integral of the rate of deformation and used together with the Cauchy stress.

Values of properties for illustration purposes are as follows: density $\rho = 7{,}800\ \text{kg/m}^3$, $E = 190\ \text{GPa}$, $\nu = 0$ or 0.3, yield stress $\sigma_Y = 316\ \text{MPa}$, and $\varepsilon^{pl} = 0.510$ at $\sigma = 616\ \text{MPa}$.

2.3 Elements

The plane strain, 4-node bi-linear CPE4R elements with reduced integration and hourglass control are used. The reduced integration uses a lower-integration for the element stiffness. The advantages of the reduced integration elements include the strain and stress calculations at the Barlow points which provide optimal accuracy, the reduction in CPU time and storage requirements from the reduced number of integration points as well as acceptable performances for approximately incompressible material behaviours. The main disadvantage is the element rank-deficient from the zero-energy modes with excessive deformations. This problem can be reduced with the hourglass control procedure which adds a small artificial stiffness.

3. Elastic Wave Propagations

In this section, the elastic wave theory is outlined and the stress wave propagations in simple geometries from uniform load pulses are simulated.

When an elastic solid is subjected to a stress pulse, the elastic stress wave propagates through the body at the sonic speed c [7],

$$c = \sqrt{\frac{E(1-\nu)}{\rho(1+\nu)(1-2\nu)}}\ \text{or}\ c = \sqrt{\frac{E}{\rho}}\ \text{when}\ \nu = 0\,. \qquad (3)$$

In wave simulations, the finite different concept is used to determine the relationship between the sizes of time increment and grids [8]. The stability consideration limits the maximum size of the time increment Δt by the Courant number Co,

$$\text{Co} = c\Delta t/\Delta x\ , \qquad (4)$$

where Δx is the smallest element size. In other words, the distance travelled by the fastest wave in the body should be smaller than the smallest typical element size in the mesh during one time step so that the wave passage through the elements can be detected.

3.1 1D Elastic Bar

When, a long elastic bar is subjected to a pressure pulse with maximum amplitude σ_p at one end, the longitudinal elastic stress wave propagates through the bar at the sonic speed c. When the wave reaches the bottom end of the bar, it reflects and travels backwards. In the simulations, the 1D mesh is obtained through constraining top and bottom sides of the bar as shown in Figure 2a.

a) 1D bar

b) 2D bar

c) thick wall

d) thin wall

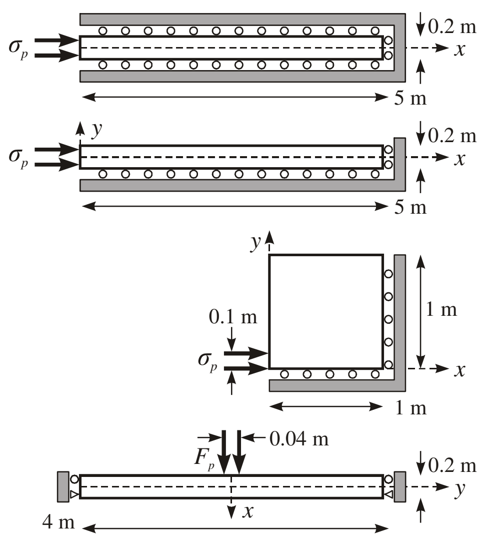

Figure 2 Problem descriptions.

First, the zero-ν, plane strain problems, with the analytical wave speed of 4935 m/s, are considered. The 4×100 elements mesh is used for the simulations with different time steps $\Delta t = 0.5$, 1, 5 and 10 μs, or equivalent to Co of 0.049, 0.099, 0.49 and 0.99, respectively.

Figure 3 shows the comparison between the analytical σ_a and numerical axial stresses from the modelling with $\Delta t = 1\,\mu s$ at various time instants. The numerical results display the classic overshoots and subsequently damping around the analytical values or the oscillatory response of stress at the shock fronts due to the inertia from sudden loading and unloading. The propagation of stress wave may be traced from the graph of maximum axial stress (Figure 4), from which the time of pulse reflection and superposition can be observed and compared with the analytical value of 1.01 ms.

Then, the size of time increment is considered. The results from simulations with $\Delta t = 1\,\mu s$ and $0.5\,\mu s$ are essentially the same, i.e. the time step independency is obtained. However, when $\Delta t = 5\,\mu s$, amplitude of the oscillating stress decreases slightly (Figure 5). Hence, the time increment of $1\,\mu s$ is recommended but the use of time step size up to $5\,\mu s$ is acceptable as the differences in stress amplitudes are quite small.

It is noted that when the time step size is still within the limit of Co = 1, the combination of sharp shock from the near-square stress pulse and associated sudden deformation destabilise the simulations, yielding the total numerical broken-down. For this problem, the limit is found to occurs at $\Delta t = 9.8\,\mu s$ or at Co = 0.97.

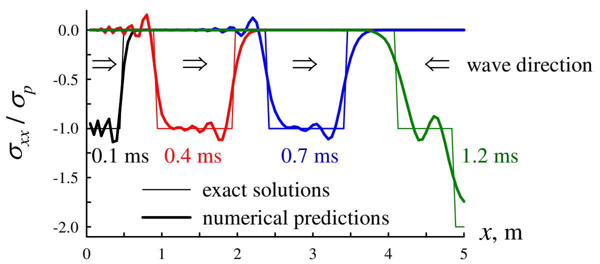

Figure 3 Elastic stress pulses from the 1D bar with 400 plane strain elements, $\nu = 0$ & Δt = 1 μs (Co ≈ 0.1).

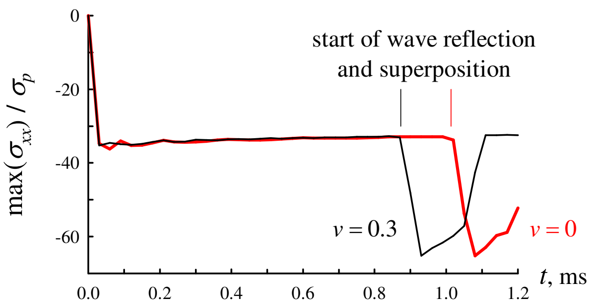

Figure 4 Maximum stress amplitudes from the 400-plane strain element model with, $\nu = 0$ & Δt = 1 μs.

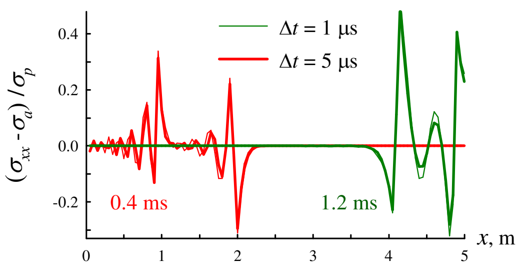

Figure 5 Stress difference comparisons from the model with 400 plane strain elements, $\nu = 0$ & Δt = 5 and 1 μs.

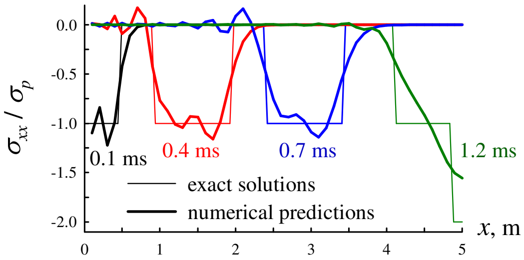

Figure 6 Elastic stress pulses from the 1D bar with 100 plane strain elements, $\nu = 0$ & Co ≈ 0.0025.

A coarse zero-ν, plane strain grid of 2×50 elements is modelled with Δt = 0.5, 0.1, and 0.05 μs, or roughly Co of 0.025, 0.0049 and 0.0025, respectively. It is found from the numerical predictions that if the mesh is too coarse, some solution features may not be captured, particularly the shock fronts, even when Co is very low (Figure 6).

Then, simulations are repeated with a non-zero ν material. The 0.3 value of Poisson's ratio ν boosts the analytical wave speed up by 16% to 5726 m/s. The overall results are very similar to the zero ν modelling but with a higher wave speed such that the stress wave arrives at the end of the bar at the time t = 0.87 ms as shown in Figure 4. It is also found that if the stress load is replaced by boundary velocity, the resulting stresses from zero and non-zero ν materials are different with axial stress in the non-zero ν material are higher by some 15%.

3.2 2D Elastic Bar

The problem is set up in the same conditions as the 1D bar with the exception of the top constraints (Figure 2b). Even though the stress wave propagation is still dominated by the axial components, the Poisson effect causes lateral expansions and contractions under a propagating pulse and generates the secondary transverse waves travelling in the bar [7].

The zero-ν, plane strain bar is first considered in the numerical simulations for the effect of Poisson's ratio. As expected, the numerical predictions are the same as those obtained from the 1D bar.

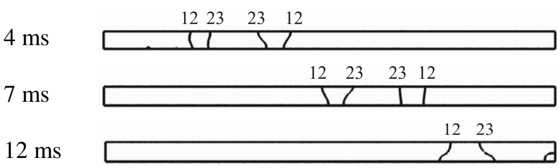

Figure 7 Stress σ_{Mises} contours (MPa) at various time t of the 2D bar with 400 elements, $\nu = 0.3$ & Δt = 1 μs.

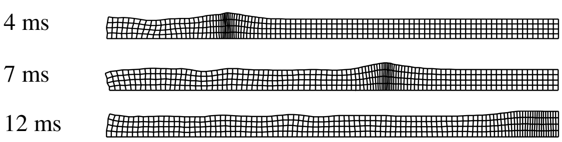

Figure 8 Exaggerated (×4000) Poisson deformation at various t of the 2D plane strain bar, $\nu = 0.3$ & Δt = 1 μs.

Then, the non zero-ν problem is investigated, employing the recommended modelling parameters in the previous section. The stress wave propagations in mainly axial directions but with some trailing lateral reflections (Figure 7) as well as the lateral deformations (Figure 8) may be observed. Figure 9 respectively shows the axial, lateral and von Mises elastic stress pulses along the bar at various time instants. Even though the early axial stress stays close to σ_p, the values roughly increase by 15% at t = 0.3 ms due to the boundary expansion of bar as whole pulses appears and becoming stabilised. In addition, the sharp axial pulse is lost and no longer closely emulates the applied near-square stress pulse. The σ_{yy} pulse dissipates very quickly as the bar is thin in that direction as well as the fact that the free end is more flexible.

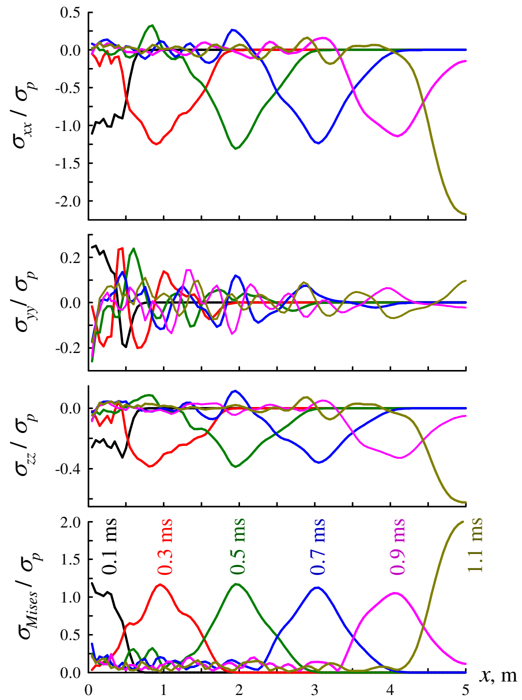

Figure 9 Elastic stresses from the 2D bar with 400 plane strain elements, $\nu = 0.3$ & $\Delta t = 1$ μs (Co ≈ 0.11).

3.3 Elastic Thick Wall

When an infinite medium is subject to a pointed near-square force pulse, the wave front propagates outwards from the disturbance source with gradually decreased amplitude as the energy is dispersed into larger regions. However, if the body is finite (Figure 2c), several types of elastic waves are generated, principally the compression, shear and Rayleigh (surface) waves [7].

A non zero-ν grid of 100×100 elements is modelled with $\Delta t = 0.5$ μs, or Co = 0.29. The stress contours are shown in Figure 10 while the stresses at y = 0 are plotted in Figure 11. It is clear from Figure 10 that the stress propagates from the source. The stresses in areas directly in front of the short applied pressure move directly forwards while the stresses at the end of the applied source spread in the semi-circle fashion. The stress amplitude decreases as the stress wave dissipates the impact energy into wider areas.

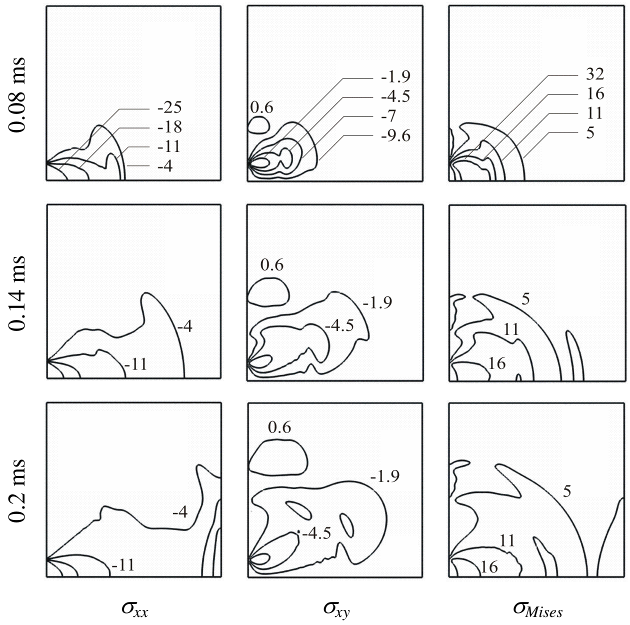

Figure 10 Stress contours (MPa) in the elastic thick wall with $\nu = 0.3$ & $\Delta t = 0.5$ μs (Co ≈ 0.29).

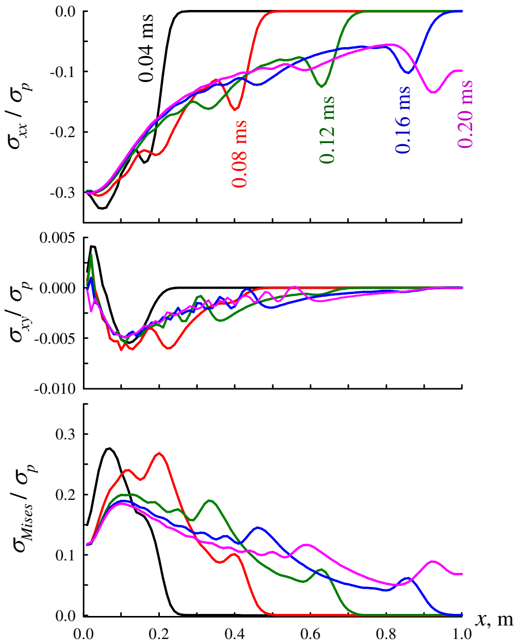

Figure 11 Stresses in the elastic thick wall with 10,000 plane strain elements, $\nu = 0.3$ & $\Delta t = 0.5$ μs (Co ≈ 0.29).

3.4 Elastic Thin Wall

When a plate is subject to a transverse load (Figure 2d), as in the ballistic impact, an extremely complicate propagation, reflection and superposition of different wave types occurs, even within an elastic solid. In practice [4], the stresses are often simplified into the transverse wave with the velocity of c_T, which is a function of shear modulus G_T and ρ,

$$c_T = \sqrt{G_T / \rho} \,. \tag{5}$$

The problem is modelled with non-zero-ν, plane strain mesh with 10×200 elements and the time step $\Delta t = 0.5$ μs or Co = 0.14. The stresses in Figure 12 show that the wave moves in the transverse direction by repeated reflecting with the boundaries of the wall. The von Mises graphs show the motion of wave fronts is just slightly slower than the approximated transverse wave speed $c_T = 3061$ m/s,

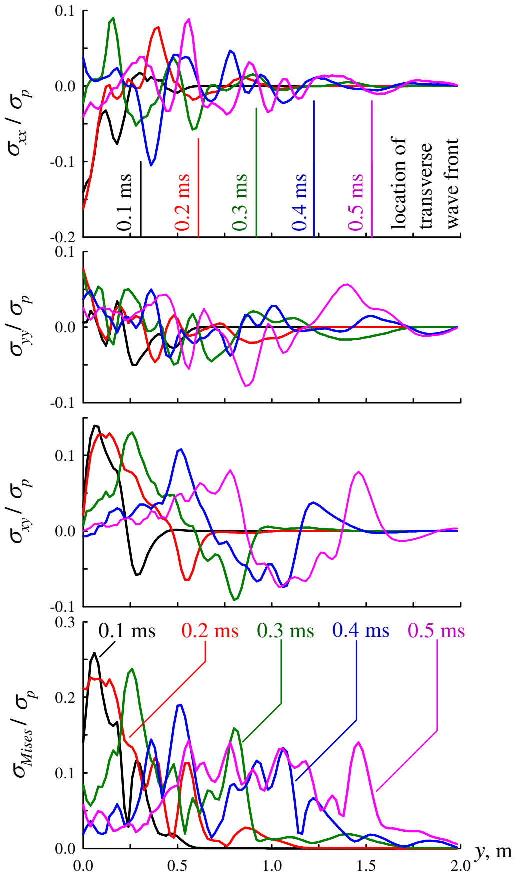

Figure 12 Stresses in the elastic thin wall with 2,000 plane strain elements, $\nu = 0.3$ & $\Delta t = 0.5$ μs (Co ≈ 0.14).

4. Elastic Plastic Wave Propagations

Simulations are repeated with elastic-plastic solids.

4.1 1D Elastic Plastic Bar

When the magnitude σ_p of the load pulse on 1D bar in section 3.1 exceeds the yield strength of the materials, the solid becomes elastic plastic and exhibit the characteristics accordingly (Figure 13). When the load is increased, the values of von Mises stress raises very slowly after it reaches the yield stress, showing as a rather flat cut-off in the graph due to the low values of plastic modulus. Even without the Poisson effect, the incompressible plastic deformation induces stresses in other directions and there is a secondary plastic-induced stress trails behind the main stress pulse.

4.2 2D Elastic Plastic Bar

The elastic plastic simulation (Figure 14) show similar characteristics as the elastic modeling, the introduction of stresses in other directions. As the plastic deformation limits the increase of von Mises stress, other stress components are relatively higher and the truncation of von Mises stress after the yielding is observed.

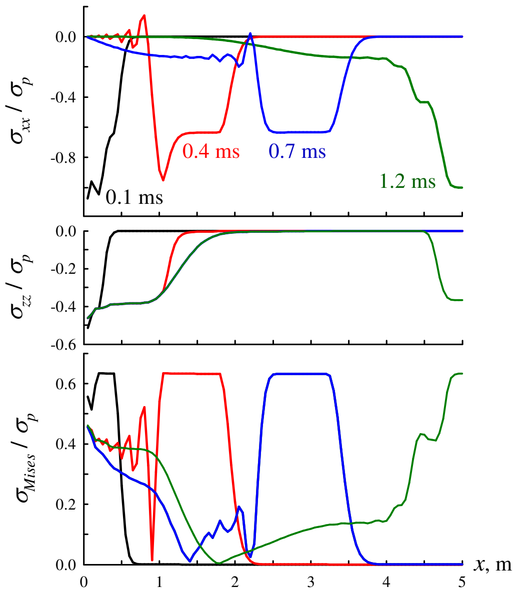

Figure 13 Elastic plastic stress pulses from 1D bar with 400 plane strain elements, $\nu = 0$ & $\Delta t = 1$ μs.

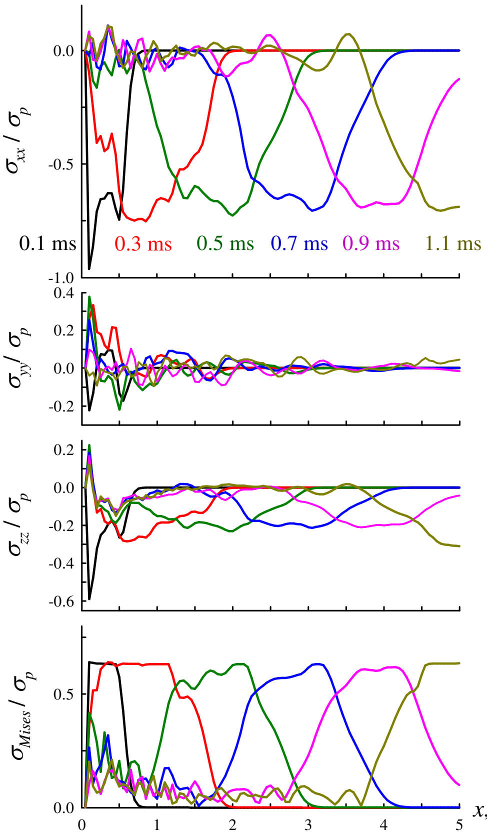

Figure 14 Elastic plastic stresses from 2D bar with 400 plane strain elements, $\nu = 0.3$ & $\Delta t = 1$ μs.

4.3 Elastic Plastic Thick Wall

As before, the plastic deformations inhibit the sharp cut-off of von Mises stress with increasing load (Figure 15). It can be seen that the plastic deformations occurs near the loads and as the wave propagates into wider regions, the stress amplitude may be reduced until only elastic deformation occurs. However, as the wave reaches the other surface, the amplitude is increased from wave superposition and plasticity may again takes place.

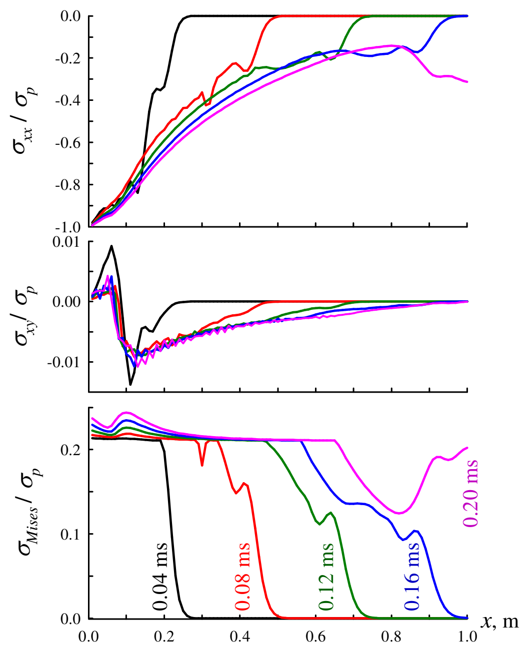

Figure 15 Stresses in the elastic plastic thick wall with $\nu = 0.3$ & $\Delta t = 0.5$ μs (Co ≈ 0.29).

4.4 Elastic Plastic Thin Wall

The stresses in the load directions are very high near the source, introducing the plasticity in that area (Figure 16). As the load is dispersed sideway, the stress amplitude reduces such that the deformation becomes wholly elastic. Yet, the localised plasticity introduces higher values of transverse stresses and the shape of stress pulses is comparatively flatten.

5. Conclusion

Elastic and elastic plastic stress wave propagations from near-square stress pulses are simulated. In all, 4 simple geometries are considered. It is clear that, apart from extremely simple problems, the stress wave propagations are very complex. The numerical method is required for the analyses with special cares on the Courant number Co selection. Even though the state of stress reaches quasi-static conditions very quickly in the order of milli-seconds, the superposition of waves at free surfaces can pose problems as the stress amplitude doubles and can cause localised failures. In armour applications, the ejection of broken pieces may prove dangerous [3] and hence, the stress waves should be taken into considerations in the armour design, both as the mean of improving energy dissipation as well as the possible source of fracture.

Acknowledgments

This research is supported by the National Metal and Materials Technology Center (MTEC), contract no. MT-B-48-CER-07-188-I. Special thanks are due to Dr. K. Sujirote, Dr. D. Atong, Dr. K. Prapakorn, Dr. A. Manonukul, Assc. Prof. Dr. T. Amornsakchai, Asst. Prof. Dr. S. Rimdusit and Maj. Gen. Dr. W. Phlawadana.

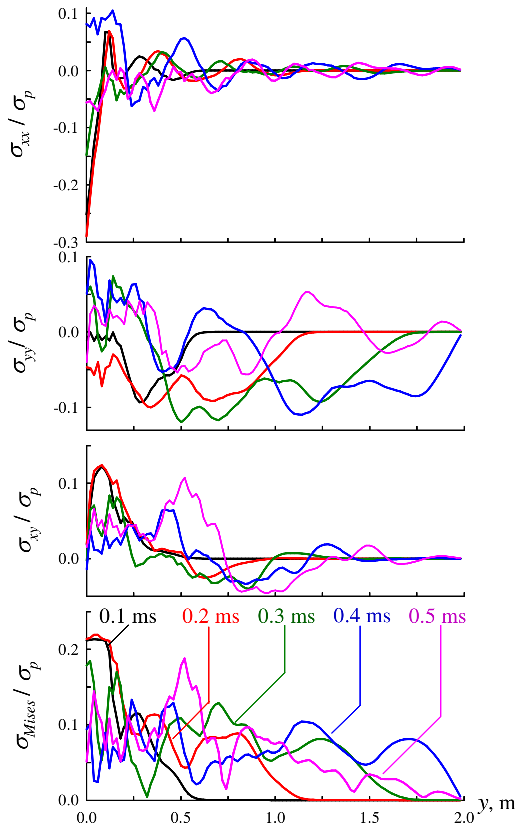

Figure 16 Stresses in the elastic plastic thin wall $\nu = 0.3$ & $\Delta t = 0.5$ μs (Co ≈ 0.14).

References

[1] K. Prapakorn, K. Maneeratana, K. Sujirote, D. Atong, T. Amornsakchai, N. Chollacoop, S. Rimdusit, and A. Manonukul, “Development of light weight hard armor for the Royal Thai Military Armory”, NSTDA Annual Conference 2005, Bangkok, 28-30 March 2005, code P030 (in Thai).

[2] P. Siribodhi, W. Wongdontri and P. Twinprawat, “Damage assessment of naval surface vessels resulted from underwater explosions”, ME-NETT 17 Conference, Pracheanburi, Thailand, 15-17 October 2003, code AM002 (in Thai).

[3] K.J.W. Goad and D.H.J. Halsey, Ammunition (Including Grenades & Mines), Brassey’s Battlefield Weapons Systems & Technology Volume III, Brassey, UK, 1982, pp. 116-118.

[4] S.S. Morye, P.J. Hine, R.A. Duckett, D.J. Carr and I.M. Ward, “Modelling of the energy absorption by polymer composites upon ballistic impact”, Composites Science and Technology, Vol. 60, 2000, pp. 2631-2642.

[5] M.J.N.Jacbos and J.L.J. van Dingenen, “Ballistic protection mechanisms in personal armour”, Journal of Material Science, Vol. 36, 2001, pp. 3137-3142.

[6] ABAQUS Inc., ABAQUS 6.3.1 Documentation, Rhode Islands, USA, 2003.

[7] K.F. Graff, Wave Motion in Elastic Solids, Oxford, Clarendon Press, 1975.

[8] K.-J. Bathe, Finite Element Procedures, Prentice-Hall, New Jersey, 1996, pp. 814-822.